New Method for Enhanced Efficiency in Detection of Gravitational Waves from Supernovae Using Coherent Network of Detectors

S. Mukherjee, L. Salazar
Center for Gravitational Wave Astronomy, Dept. of Physics and Astronomy,
*The University of Texas at Brownsville, One, West University Boulevard, Brownsville, TX 78520, U.S.A.**

Supernovae in our universe are potential sources of Gravitational Waves (GW) that could be detected in a network of Gravitational Wave (GW) detectors like LIGO, Virgo, and GEO600. Core-collapse supernovae are very rare, but the associated gravitational radiation is likely to carry profuse information about the underlying processes driving the supernovae. Calculations based on analytic models predict GW energies within the detection range of the Advanced LIGO detectors, out to tens of Mpc. The signals from these sources are weak and rare. Thus, methods that can improve the sensitivity of searches for GW signals from supernovae are desirable, especially in the advanced detector era. Several methods have been proposed based on various likelihood-based regulators that work on data from a network of detectors to detect burst-like signals (as is the case for signals from supernovae) from potential GW sources. To address this problem, we have developed an analysis pipeline based on a method of noise reduction known as the Harmonic Regeneration Noise Reduction (HRNR) algorithm. Sixteen supernova waveforms from the Murphy et al. 2009 catalog have been used in presence of LIGO science data. A comparative analysis is presented to show detection statistics for a standard network analysis as commonly used in GW pipelines and the same by implementing the new method in conjunction with the network. The result shows improvement in detection statistics by a factor of at least 30% even for very weak signal to noise ratios (snr). The improvement in the detection statistics grows steadily with increasing snr's.

PACS numbers: 95.85.Sz,04.80.Nn, 07.05.Kf, 02.50.Tt, 02.60.Pn

I. INTRODUCTION

Supernovae in our universe are potential sources of Gravitational Waves (GW) [1–3] that could be detected in a network of Gravitational Wave (GW) detectors like LIGO [4], Virgo [5], and GEO600 [6]. Core-collapse supernovae are very rare, but the associated gravitational radiation is likely to carry profuse information about the underlying processes driving the supernovae. Calculations based on analytic models predict GW energies within the detection range of the Advanced LIGO [7] detectors, out to tens of Mpc.

The GW frequency from neutrino driven core collapse supernovae [11] evolves from approximately100 Hz to about 400 Hz. The higher frequencies correspond to higher mass progenitors and] longer explosion time by the neutrino mechanism. The GW strain amplitude increases about 10 times with the vigorous convective motion." During explosion, the high frequency signal dies down and is replaced by low frequencies in the range of tens of Hz. Since the current detectors have, in principle, the ability to detect signals ≥ 50 Hz, it is worthwhile to develop an efficient method to search these signals in the detector data. The explosion stageleads to a reduction of detectable GW emission. But for the stages before explosion, GW emission can be modeled with characteristic frequencies and amplitudes.

Since the signals from these sources are weak and rare, methods that can improve the sensitivity of searches for GW signals from supernovae are desirable, especially in the advanced detector era. Several methods have been proposed [8–10] based on various likelihood-based regulators that work on data from a network of detectors to detect burst-like signals (as is the case for signals from supernovae) from potential GW sources. To address this problem, we have developed a new method of noise reduction based on Harmonic Regeneration Noise Reduction (HRNR) algorithm [12–15].

The paper is organized as follows. Section II describes the algorithm development in detail. Section III describes the analysis pipeline where sixteen supernova waveforms from the Murphy et al. 2009 catalog [11] have been used in presence of LIGO science data. A comparative analysis is presented to show detection statistics for a standard network analysis as commonly used in GW pipelines and the same by implementing the new method in conjunction with the network. Section IV discusses the results and section V summarizes the conclusion.

II. METHOD

The basic problem can be stated as follows. We assume an additive noise model.

$$x(t) = s(t) + n(t) \tag{1}$$

where $x(t)$ is the data stream, $s(t)$ is the signal, embedded in noise $n(t)$. The corresponding k^{th} spectral

*Corresponding author:soma@phys.utb.edu

components of a small segment p are $X(p,k)$, $S(p,k)$ and $N(p,k)$.

Our aim is to find find an estimator $\tilde{S}(p,k)$ such that expectation value of distortion based on spectral noisy features is minimized.

Since we do not have a readily available spectral estimate, we begin by estimating the signal-to-noise ratio (snr) from the noisy data.

An estimate of $S(p,k)$ is then obtained by applying a spectral gain $\Gamma(p,k)$ to each short-time spectral component $X(p,k)$. The choice of the distortion measure determines the gain behavior, i.e., the tradeoff between noise reduction and signal distortion. However, the key parameter is the estimated snr because it determines the efficiency of the signal enhancement for a given noise power spectrum density (psd).

Most of the classic signal enhancement techniques require the evaluation of two parameters: the *a posteriori* snr and the *a priori* snr, respectively defined by

$$snr_{post}(p,k) = \frac{|X(p,k)|^2}{E[|N(p,k)|^2]} \tag{2}$$

and

$$snr_{priori}(p,k) = \frac{E|S(p,k)|^2}{E[|N(p,k)|^2]} \tag{3}$$

We also define the *instantaneous* snr as follows.

$$snr_{ins}(p,k) = \frac{|X(p,k)|^2 - E[|N(p,k)^2|]}{E[|N(p,k)|^2]} \tag{4}$$

In reality, $E[|N(p,k)^2|$ and $E[|S(p,k)^2|$ are both unknown and need to be estimated. $E[|N(p,k)^2|$ (written as $\tilde{\zeta}(p,k)$ from now onwards) can be estimated by the classical recursive methods [13].

The spectral gain is obtained as follows.

$$\Gamma(p,k) = f(s\tilde{n}r_{prior}(p,k), s\tilde{n}r_{post}(p,k)) \tag{5}$$

The function f is chosen in this case to be a Wiener filter. The signal spectrum $E[|S(p,k)^2|$ can then be estimated as follows.

$$\tilde{S}(p,k) = \Gamma(p,k)X(p,k) \tag{6}$$

A. *a priori* and *a posteriori* snr

We would derive the relation between the *a priori* and *a posteriori* snr.

Assuming the model given in equation [1], the amplitude of the noisy signal is given by,

$$|X(p,k)| = \left(|S(p,k)|^2 + |N(p,k)|^2 + 2|S(p,k)||N(p,k)|cos\beta(p,k)\right)^{\frac{1}{2}} \tag{7}$$

where $\beta(p,k)$ is the phase angle between $S(p,k)$ and $N(p,k)$.

Let us define a local *a priori* and *a poteriori* snr as follows.

$$snr^{local}_{post}(p,k) = \frac{|X(p,k)|^2}{|N(p,k)|^2} \tag{8}$$

and

$$snr^{local}_{priori}(p,k) = \frac{|S(p,k)|^2}{|N(p,k)|^2} \tag{9}$$

Using equation [7] in equation [8], we get

$$snr^{local}_{post}(p,k) = 1 + snr^{local}_{priori}(p,k) + 2\sqrt{snr^{local}_{priori}(p,k)} \times cos\beta(p,k) \tag{10}$$

For Wiener filter, $\beta(p,k) = \pi/2$.

III. DECISION DIRECTED APPROACH

1. Principle

Using the noise psd, the *a priori* and *a posteriori* snrs are computed as follows.

$$s\tilde{n}r_{post}(p,k) = \frac{|X(p,k)|^2}{\tilde{\zeta}(p,k)} \tag{11}$$

and

$$s\tilde{n}r^{DD}_{prior}(p,k) = \epsilon\frac{|\tilde{S}(p-1,k)|^2}{\tilde{\zeta}(p,k)} + (1-\epsilon)P[s\tilde{n}r_{post}(p,k) - 1) \tag{12}$$

where $\tilde{S}(p-1,k)|$ stands for estimated signal spectrum at the previous frame and $P[s\tilde{n}r_{post}(p,k) - 1)$ is the half wave rectification. ϵ is closen to be 0.98. The above estimate is known as Decision Directed approach [14]. With the spectral gain being chosen as the Wiener filter, we have

$$\Gamma_{DD}(p,k) = \frac{s\tilde{n}r^{DD}_{prior}(p,k)}{1 + s\tilde{n}r^{DD}_{prior}(p,k)} \tag{13}$$

2. Consequences

Two observations are important here: (i) when the instantaneous snr is $>> 0$ *db*, $snr_{prior}(p,k)$ corresponds to a frame delayed version of the instantaneous snr; (ii) when the instantaneous snr is < 0 *db*, $snr_{prior}(p,k)$ corresponds to a highly smoothed and delayed version of

instantaneous snr. This means that the variance of the *a priori* snr is reduced compared to the instantaneous snr. The direct effect of this phenomenon is the reduction of underlying noise to effectively enhance the signal [15]

It is to be noted that the delay inherent to the DD algorithm is a drawback especially in the beginning and end of the signal. Furthermore, this delay introduces a bias in gain estimation which limits noise reduction performance and generates a reverberation effect.

IV. TWO STEP NOISE REDUCTION TECHNIQUE

In order to avoid some of the problems faced in the estimation of the *a priori* snr, a two step noise reduction (TSNR) technique has been developed. The DD algorithm introduces a frame delay when ϵ is ~ 1. As a result of this, the spectral gain matches the values in the p^{th} and the $(p-1)^{th}$ frame. We now adopt a two step approach by applying the DD algorithm to the $(p+1)^{th}$ frame too. In this approach, we first calculate spectral gain as given by equation [13]. In the next step, this gain is used to calculate the *a priori* snr in the $(p+1)^{th}$ frame. The gain factor is given by

$$\tilde{s}nr^{TSNR}_{prior}(p,k) = \tilde{s}nr^{DD}_{prior}(p+1,k). \tag{14}$$

Hence,

$$\tilde{s}nr^{TSNR}_{prior}(p,k) = \frac{|\Gamma_{DD}(p,k)X(p,k)|^2}{\tilde{\zeta}(p,k)}. \tag{15}$$

Finally, the spectral gain is calculated as follows.

$$\Gamma_{TSNR}(p,k) = \frac{snr^{TSNR}_{prior}(p,k)}{1+snr^{TSNR}_{prior}(p,k)} \tag{16}$$

and hence the enhanced signal estimate is

$$\tilde{S}(p,k) = \Gamma_{TSNR}(p,k)X(p,k). \tag{17}$$

To summarize, the TSNR algorithm improves the noise reduction performance since the gain matches to the current frame whatever the snr. The main advantages of this approach are the ability to preserve the beginning and end of the signal's onset and offset, and to successfully remove the reverberation effect typical of the DD approach. In practice this reverberation effect can be reduced by increasing the overlap between successive frames but cannot be suppressed whereas the TSNR approach makes it possible with a typical overlap of 50 %.

A. Theoretical explanation

If no speech is present in the $(p-1)^{th}$ frame,

$$\tilde{S}(p-1,k) = 0. \tag{18}$$

At the p^{th} frame, the DD approach gives the estimation for *a priori* snr as

$$\tilde{s}nr^{DD}_{prior}(p,k) = (1-\epsilon)P(\tilde{s}nr_{post}(p,k)-1). \tag{19}$$

When refining the *a priori* snr in the TSNR technique, according to equation [15] (using equations [11 and 13],

$$\tilde{s}nr^{TSNR}_{prior}(p,k) = \left[\frac{(1-\epsilon)P(\tilde{s}nr_{post}(p,k)-1)}{1+(1-\epsilon)P(\tilde{s}nr_{post}(p,k)-1)}\right]^2 \times snr_{post}(p,k). \tag{20}$$

By comparing equations [19 and 20], we find that

$$\tilde{s}nr_{post}(p,k) > \frac{1}{2\epsilon}\left[1+2\epsilon+\sqrt{\frac{1+3\epsilon}{1-\epsilon}}\right] \tag{21}$$

It is evident from the above equation that the TSNR method delivers a greater signal power than the DD algorithm. Consequently, if a signal component appears abruptly at frame p , thus increasing the *a posteriori* snr, the estimated *a priori* snr tends to the *a posteriori* snr suppressing the bias introduced by the DD approach. This bias decreases when the *a posteriori* snr increases. However, if signal is absent at frame p too, keeping the *a posteriori* snr to a low level, the estimated *a priori* snr becomes lower than for the DD approach further limiting the noise.

Looking at the other extreme case, where *a priori* snr is higher in $(p-1)^{th}$ frame than in the p^{th} frame (i.e. the signal decays rapidly), the following approximation can be done.

$$\tilde{s}nr^{DD}_{prior}(p,k) \sim \epsilon\tilde{s}nr_{instantaneous}(p-1,k) \tag{22}$$

The sepctral gain is then approximated as follows.

$$\Gamma_{DD}(p,k) = \frac{\epsilon\tilde{s}nr_{instantaneous}(p-1,k)}{1+\epsilon\tilde{s}nr_{instantaneous}(p-1,k)} \tag{23}$$

Moreover, it is reasonable to assume that $\tilde{s}nr_{instantaneous}(p-1,k)$ 1 and is much greater than 1 and $\epsilon \sim 1$, equationn [23] becomes

$$\Gamma_{DD}(p,k) \sim 1. \tag{24}$$

Inducting this approximation in [15] leads to

$$\tilde{s}nr^{TSNR}_{prior}(p,k) \sim \tilde{s}nr_{post}(p,k) \sim \tilde{s}nr_{instantaneous}(p,k). \tag{25}$$

The TSNR method leads to suppresion of *a priori* snr overestimation.

V. HARMONIC REGENERATION NOISE REDUCTION

The Harmonic Regeneration Noise Reduction (HRNR) consists of applying a nonlinear function to the time signal enhanced in the process described in the previous section. The restored signal is given by

$$S_{restored}(t) = \Phi(\tilde{s}(t)), \tag{26}$$

where Φ is the nonlinear function.The maximum value relative to zero has been used in this case.

It is important to note that the $S_{restored}(t)$ are created at the same positions as the original signal, thus *no distortions are produced*. Moreover, it contains a useful information that leads to a further refinement in the *a priori* snr estimate as follows.

$$\begin{aligned}\tilde{snr}_{prior}^{HRNR}(p,k) = \frac{1}{\tilde{\zeta}(p,k)} \times (\Delta(p,k)|\tilde{s}(p,k)|^2 \\ +(1-\Delta(p,k))|S_{restored}(p,k)|^2).\end{aligned} \tag{27}$$

The $\Delta(p,k)$ is a mixing parameter.

$$0 \leq \Delta(p,k) \leq 1. \tag{28}$$

We will use

$$\Delta(p,k) = \Gamma_{TSNR}(p,k). \tag{29}$$

This ensures that when the estimate obtained from [25] is a reliable estimate, the $|Delta(p,k) = 1$. However, if the estimate is not a reliable one, the $|Delta(p,k) = 0$. A standard value, e.g.0.5, can also be used in some cases.

The refined *a priori* snr from equation [27] is now used to calculate the new spectral gain *with preservation of all features of the original signal*. As before, we have chosen the spectral gain to be the Wiener filter. Thus,

$$\Gamma_{HRNR}(p,k) = \frac{\tilde{snr}_{prior}^{HRNR}(p,k)}{1+\tilde{snr}_{prior}^{HRNR}(p,k)}. \tag{30}$$

At the final stage, the desired signal spectrum is given by,

$$\tilde{\mathbf{S}}(p,k) = \Gamma_{HRNR}(p,k)X(p,k) \tag{31}$$

A. Theoretical explanation of HRNR

As stated in the previous section, we choose the nonlinear function Φ as follows.

$$S_{restored}(t) = Max[\tilde{s}(t),0] = \tilde{s}(t) \times \rho(\tilde{s}(t)), \tag{32}$$

where ρ is defined as

$$\begin{aligned}\rho(f) = 1 \ \text{ if } \ f > 0 \\ \rho(f) = 1 \ \text{ if } \ f < 0.\end{aligned} \tag{33}$$

It is reassonable to assume that, over a short time period, the signal is quasistationary. The fourier transform (FT) of $\rho(f)$ is given by,

$$\tilde{\rho}(\tilde{s}(t)) = \frac{1}{T}\sum_{n=-\infty}^{\infty} K(\frac{n}{T})\delta(\nu - \frac{n}{T}), \tag{34}$$

where δ is the Dirac delta function and ν denotes the frequency. $K(\frac{n}{T})$ is the FT of the underlying elementary waveform at discrete frequency $\frac{n}{T}$. Using [31], the FT of $S_{restored}(t)$ is given by,

$$\begin{aligned}\tilde{S}_{restored}(t) = FT(\tilde{s}(t)) \times \frac{e^{-i\theta}}{T} \\ \times \sum_{n=-\infty}^{\infty} K(\frac{n}{T})\delta(\nu - \frac{n}{T}).\end{aligned}$$

θ is the phase angle at the origin. In summary, the spectrum of the restored signal is the convolution between the signal enhanced by the TSNR and a harmonic comb with the same freqeuncy as the signal.

VI. ANALYSIS

A. Data used

Sixteen supernova waveforms from the Murphy et al. 2009 catalog [11] have been used in presence of LIGO fourth science run (S4 [16]) data for demonstration of results from the search algorithm. The catalog describes the GW signals from neutrino driven core collapse supernovae. The waveforms used in the study are shown in figure 1.

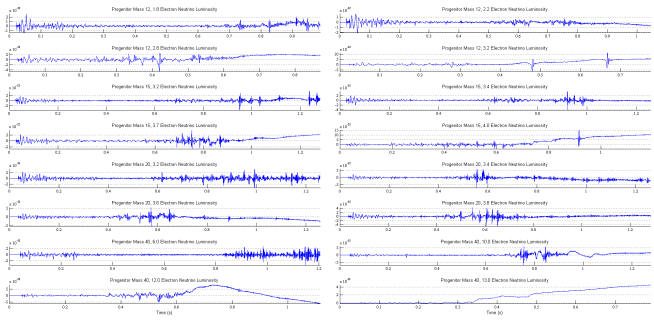

FIG. 1: The figure shows the supernovae waveforms used in the study from the Murphy etal. 2009 catalog [11].

The analysis pipeline is shown in figure 2.

Sets of test data, each 60 seconds long) from the main GW channel (DARM_ERR) from the two Hanford detectors (H1 and H2) and the Louisiana detector (L1) are used for demonstration of results. The data streams have been injected with the signal waveforms. The signals

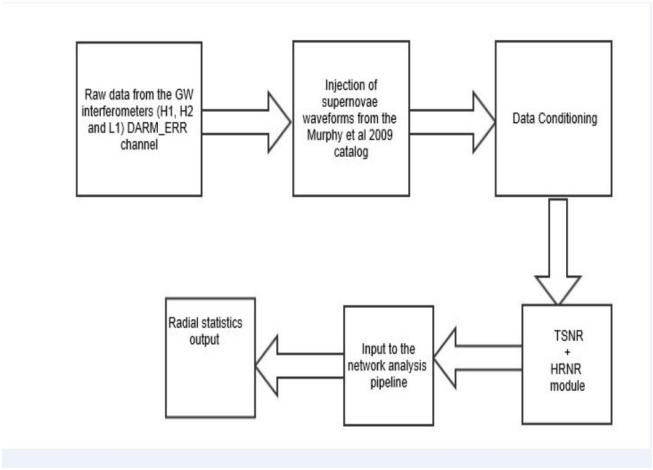

FIG. 2: The analysis pipeline starts with obtaining the raw data from the three LIGO detectors (H1: Hanford 4k, H2: Hanford 2K and L1: Livingstion 4k.) Supervovae signals are added to the data stream. The prepared data are now subjected to the data conditioning step where the data are bandpassed between 50 Hz and 2048 Hz and all narrowband noise in this range is suppressed. The conditioned data now passes thrpough the TSNR and HRNR module. The output from this module is supplied as the input to the network analysis pipeline. The network analysis pipeline yields the detection statistics in accordance with equation 36.

were introduces in the data streams starting at 10 seconds. After this, data conditioning was applied to the data containing the signal. The data conditioning consists of the following steps. (i) Extraction of raw GW channel data, centered around the trigger (extracted time series noted by, say, T0; (ii) Whitening T0 [18] and dynamically removing [19, 20] the narrowband noise present in T0; The resulting time series is denoted by cT0; (iii) Filtering cT0 with a bandwidth of 50 Hz and 2048 Hz; The resulting time series is denoted by fcT0; (iv) Resampling fcT0 to represent the appropriate band- width.

The conditioned data sets are then applied to the input of the TSNR+HRNR denoising stage. The denoised output from the TSNR+HRNR module is then used as the input to a network analysis based on regularized maximum likelihood [8–10, 17].

B. Detection statistics

It is known that the detector response to GW signal is a linear combination of the unknown polarization waveforms $h_+(t)$ and $h_\times(t)$ arriving from a direction with polar angle θ_0 and azimuthal angle ϕ_0 in an earth-centered, ecliptic reference frame.

The output of the network algorithm for a given sky location θ_0 and azimuthal angle ϕ_0 , is the value of the likelihood of the data maximized over all possible $h_+(t)$ and $h_\times(t)$ waveforms. A skymap is said to be constructed with the maximum likelihood values obtained as a function of θ_0 and azimuthal angle ϕ_0. The detection statistic is constructed from the skymap as follows.

$$R_{rad} = [(\frac{max_{\theta_0,\phi_0}\mathbf{S}(\theta_0,\phi_0)}{max_{\theta_0,\phi_0}\mathbf{S_0}(\theta_0,\phi_0)} - 1)^2 + (R_{mm} \times \frac{min_{\theta_0,\phi_0}\mathbf{S_0}(\theta_0,\phi_0)}{max_{\theta_0,\phi_0}\mathbf{S_0}(\theta_0,\phi_0)} - 1)^2]^{\frac{1}{2}}, \quad (36)$$

where R_{mm} is given by

$$R_{mm} = \frac{max_{\theta_0,\phi_0}\mathbf{S}(\theta_0,\phi_0)}{min_{\theta_0,\phi_0}\mathbf{S}(\theta_0,\phi_0)}, \quad (37)$$

and $\mathbf{S_0}$ is the expectation value of $\mathbf{S}$ when no signal is present in the data. R_{rad} is known as the radial statistics. It denotes the radial distance of the observed values in the $(R_{mm}, max_{\theta_0,\phi_0}\mathbf{S}(\theta_0,\phi_0)$ plane from the mean location in absence of the signal. The larger the radial distance, the higher is the detection probability.

C. Results

Figures 3 and 4 show the analysis results for one of the catalog waveforms (grw_12_2; progenitor mass 12, electron neutrino luminosity 2.2) injected into the data stream with a scale factor of 30, i.e. the original signal was multiplied by a factor of 30. Figure 3 shows the signal strength injected into the detector noise. For reference, a scale factor of 30 corresponds to the snr threshold below which the signal is not discerned in the network analysis radial distance statistics without the application of the TSNR+HRNR denoising module. Figure 4 top row shows the the spectrograms of the signal+noise data after being conditioned without the TSNR+HRNR denoising effect (left panel) and the same with the inclusion of the TSNR+HRNR denoising (right panel.) It is clear even visually that the TSNR+HRNR denoising efectively has enhanced the snr of the embedded signal. The bottom row shows the radial statistics (as given in equation [36]) for the analysis performed without the proposed denoising (left panel) and with the TSNR+HRNR denoising (right panel.) In the first case, the max value of R_{rad} is around 0.4, while in the second case, it is about 5.5, an improvement of a factor of 14. It may be noted that the noise scatter is much less in the second case than the firts one.

As another exmaple, figures 5 and 7 show the analysis results for one of the catalog waveforms (grw_15_3, progenitor mass 15, electron neutrino luminosity 3.2) injected into the data stream with a scale factor of 30, i.e. the original signal was multiplied by a factor of 35. Figure 5 shows the signal strength injected into the detector noise. Figure 7 top row shows the the spectrograms of the signal+noise data after being conditioned without the TSNR+HRNR denoising effect (left panel) and the same with the inclusion of the TSNR+HRNR

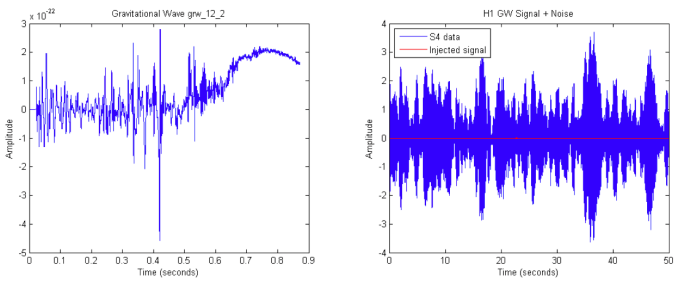

FIG. 3: The waveforms (grw_12_2 , left panel) is injected into the data stream (right panel) with a scale factor of 30. The x-axis represents time in seconds and the y-axis is the amplitude.

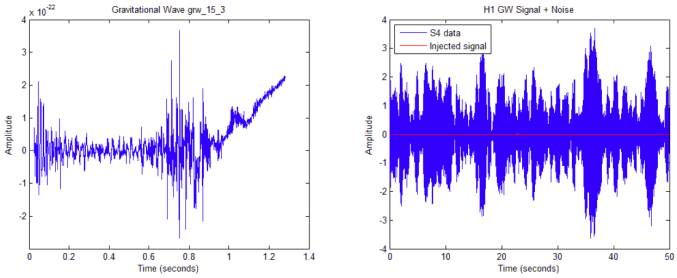

FIG. 5: The waveforms (grw_15_3 , left panel) is injected into the data stream (right panel) with a scale factor of 35. The x-axis represents time in seconds and the y-axis is the amplitude.

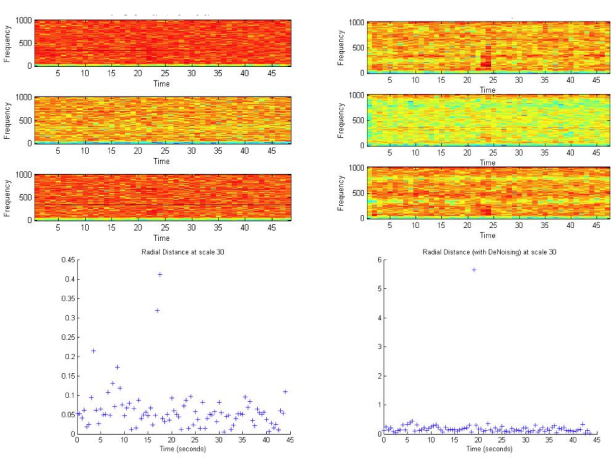

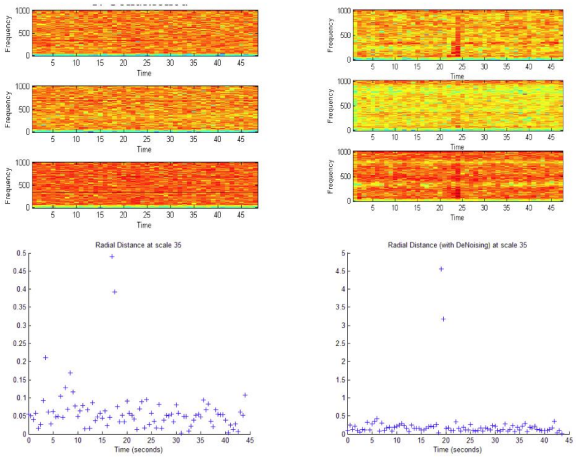

FIG. 6: The figure shows the the spectrograms of the signal (grw_15_3) +noise data after being conditioned without the TSNR+HRNR denoising effect (top left panel) and the same with the inclusion of the TSNR+HRNR denoising (top right panel.) The x-axis represents time in seconds and the y-axis represents frequency in Hz. The bottom row of figures shows the radial statistics (as given in equation [36]) for the analysis performed without the proposed denoising (left panel) and with the TSNR+HRNR denoising (right panel.) The x-axis represents time in seconds and the y-axis represents the radial distance.

denoising (right panel.) It is clear even visually that the TSNR+HRNR denoising efectively has enhanced the snr of the embedded signal. The bottom row shows the radial statistics (as given in equation [36]) for the analysis performed without the proposed denoising (left panel) and with the TSNR+HRNR denoising (right panel.) In the first case, the max value of R_{rad} is around 0.5, while in the second case, it is about 4.7, an improvement of a factor of 9.4. This conclusively shows that the extra denoising step introduced in the analysis through implementation of the TSNR+HRNR module is highly effective. This chain of analysis has been performed on all the sixteen waveforms mentioned above and the same effect has been observed.

Figures 8 and 9 show the operating characteristics, i.e. detection statistics (R_{rad}) as a function of the signal strength, measured in terms of the scale factor for the sixteen waveforms used in this study. The analysis has been carried out using signals of a wide range of strengths, starting with a very low threshold (low scale factor) up to moderately strong signals, i.e. scale factors up to 60. The detection statistics has been calculated in each case. As is evident, in all sixteen cases, the detection statistics for the current analysis with TSNR+HRNR denoising is is higher by a factor of ten or more than the cases without the application of this additional step of denoising. This is true even for weak signal strengths. This is particularly apparent in certain types of waveforms

VII. CONCLUSION

The result shows improvement in detection statistics by a factor of 10 even for very weak signal to noise ratios (snr). The improvement in the detection statistics grows steadily with increasing signal to noise ratios. HRNR significantly improves the detection statistics of GW signals from supernovae even for very weak signals. HRNR

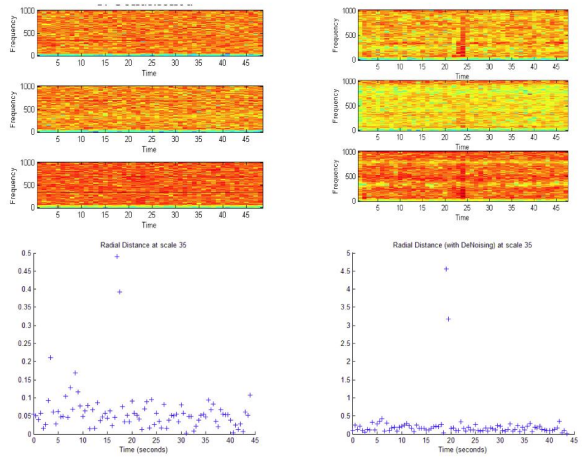

FIG. 7: The figure shows the the spectrograms of the signal (grw_15_3) +noise data after being conditioned without the TSNR+HRNR denoising effect (top left panel) and the same with the inclusion of the TSNR+HRNR denoising (top right panel.) The x-axis represents time in seconds and the y-axis represents frequency in Hz. The bottom row of figures shows the radial statistics (as given in equation [36]) for the analysis performed without the proposed denoising (left panel) and with the TSNR+HRNR denoising (right panel.) The x-axis represents time in seconds and the y-axis represents the radial distance.

works robustly even with non-stationary, non-gaussian noise. A major advantage of the proposed method is that it is a stand-alone MATLAB [21] code module that can be easily plugged in to existing search pipelines without having to make alterations. HRNR contains adjustable parameters that can in principle improve the results even more.

More extensive testing with S6 data is underway. Immediate future study includes integration of this method to existing coherent wave burst (cWB)-based [22] supernova search pipeline. More supernova signals will be incorporated in the study. It will indeed be interesting to note if the improvement in detection statistics noted in this study also remains persistent in the future studies as the advanced LIGO [**?**] becomes a reality.

VIII. ACKNOWLEDGMENT

This work is supported by NSF award number NSF PHY 1205585 (2012).

[1] C. D. Ott, E. Abdikamalov, E. O'Connor, C. Reisswig, R. Haas, P. Kalmus, S. Drasco, A. Burrows, E. Schnetter, Correlated Gravitational Wave and Neutrino Signals from General-Relativistic Rapidly Rotating Iron Core Collapse, Phys. Rev. D. 86, 024026, 2012

[2] Christian D. Ott, Christian Reisswig, Erik Schnetter, Evan O'Connor, Ulrich Sperhake, Frank Lffler, Peter Diener, Ernazar Abdikamalov, Ian Hawke, and Adam Burrows, Dynamics and Gravitational Wave Signature of Collapsar Formation, Phys. Rev. Lett., 106, 161103, 2011

[3] Ernazar Abdikamalov, Christian D. Ott, Luciano Rezzolla, Luc Dessart, Harald Dimmelmeier, A. Marek, and H.-T. Janka, Axisymmetric General Relativistic Simulations of the Accretion-Induced Collapse of White Dwarfs, Phys. Rev. D. 88, 044012, 2010

[4] A. Abramovici, W. Althouse, R. Drever, Y. Gursel, S. Kawamura, F. Raab, D. Shoemaker, L. Sievers, R. Spero, K. Thorne, R. Vogt, R. Weiss, S. Whitcomb, and M. Zucker. Science, 256:325333, 1992.

[5] T. Accadia, F. Acernese, F. Antonucci, et al., Status and perspectives of the Virgo gravitational wave detector, Journal of Physics: Conference Series 203, 2010

[6] H. Grote, K. Danzmann, K.L. Dooley, R. Schnabel, J. Slutsky, H. Vahlbruch First Long-Term Application of Squeezed States of Light in a Gravitational-Wave Observatory, Phys. Rev. Lett. 110, 181101, 2013

[7] Gregory M Harry (for the LIGO Scientific Collaboration) Advanced LIGO: the next generation of gravitational wave detectors, Class. Quantum Grav. 27, 2010

[8] S. Mohanty et al, Penalized Likelihood, CQG 23 4799, 2006

[9] M. Rakhmanov, Rank deficiency of network matrix, CQG 23 S673, 2006

[10] Sergei Klimenko, Soumya D. Mohanty, Malik Rakhmanov, Guenakh Mitselmakher, Constraint likelihood analysis for a network of gravitational wave detectors, Phys. Rev. D 72 122002, 2005

[11] Jeremiah W. Murphy, Christian D. Ott, Adam Burrows, A Model for Gravitational Wave Emission in Neutrino-Driven Core-Collapse Supernovae, Astrophysical Journal, 707, 1173, 2009

[12] Cyril Plapous, Claud Marro and Pascal Scalart, Improved Signal-to-Noise Ratio Estimation for Speech Enhancement, IEEE Transactions on Audio Speech and Language Processing, Vol. 14, 2006

[13] P. Scalart and J. Vieira Filho, Speech enhancement based on a priori signal to noise estimation, in Proc. IEEE Int. Conf. Acoust., Speech, Signal Process., Atlanta, GA, May 1996, vol. 2, pp. 629632.

[14] Y. Ephram and D. Malah, Speech enhancement using a minimum mean-square error short-time spectral amplitude estimator, IEEE Trans. Acoust., Speech, Signal Process., vol. ASSP-32, no. 6, pp. 11091121, Dec. 1984.

[15] O. Capp, Elimination of the musical noise phenomenon with the Ephram and Malah noise suppressor, IEEE Trans. Speech Audio Process., vol. 2, no. 2, pp. 345S349, Apr. 1994.

[16] B. Abbott et al. (LIGO Scientific Collaboration), All-sky search for periodic gravitational waves in LIGO S4 data,

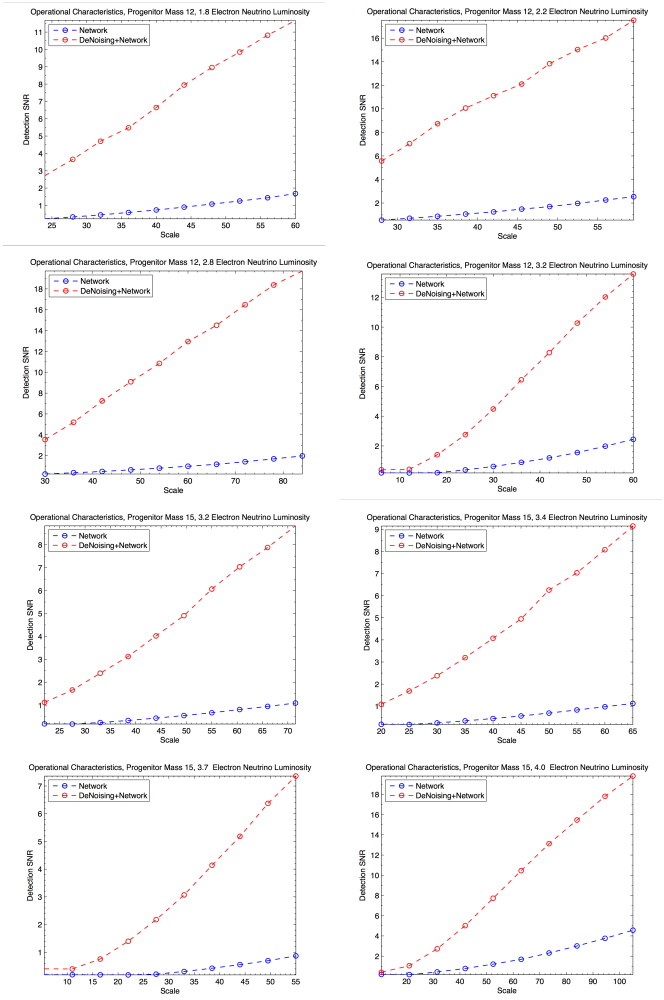

FIG. 8: The figure shows the radial statistics as a function of the injected signal strength for eight waveforms from the catalog. The x-axis represents the snr. The y-axis represents the radial distance, R_{rad}. The lower curve (in blue) is the operating characeristic for the original pipeline without the implementation of the proposed TSNR+HRNR denoising module. The upper curve (in red) represents the same with the incorporation of the TSNR+HRNR denoising.

Phys. Rev. D 77, 022001, 2008

[17] K. Hayama, S. D. Mohanty, M. Rakhmanov and S. Desai, Coherent network analysis for triggered gravitational wave burst searches, Class. Quantum Grav. 24, 2007.

[18] S. D. Mohanty, Median based line tracker (MBLT): model independent and transient preserving line removal from interferometric data, Class. Quant. Grav. 19, 1513, 2002.

[19] L. S. Finn and S. Mukherjee, Data conditioning for gravitational wave detectors: A Kalman filter for regressing suspension violin modes, Phys. Rev. D 63, 062004, 2001.

[20] A. Sintes and B. F. Schutz,Removing non-stationary, non-harmonic external interference from gravitational wave interferometer data, Phys. Rev. D 60, 062001, 1999.

[21] www.mathworks.com

[22] S. Klimenko, S., I. Yakushin, A. Mercer, et al., Coherent method for detection of gravitational wave bursts , Class.Quant.Grav. 25, 114029, 2008.

[23] G M Harry (for the LIGO Scientific Collaboration), Advanced LIGO: the next generation of gravitational wave detectors, Class. Quantum Grav. 27 084006, 2010.

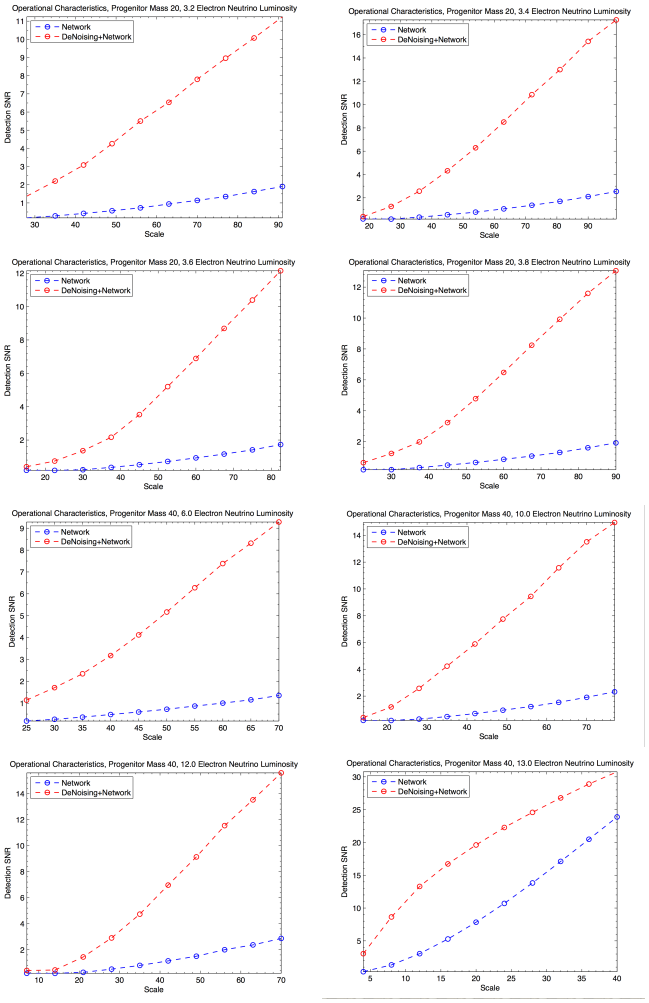

FIG. 9: The figure shows the radial statistics as a function of the injected signal strength for the remaining eight waveforms from the catalog. The x-axis represents the snr. The y-axis represents the radial distance, R_{rad}. The lower curve (in blue) is the operating characeristic for the original pipeline without the implementation of the proposed TSNR+HRNR denoising module. The upper curve (in red) represents the same with the incorporation of the TSNR+HRNR denoising.